文章编号：1001－9014(2017)02－0129－06

DOI:10.11972/j.issn.1001－9014.2017.02.001

A prototype photon detector based on interband transition of quantum wells

LIU Jie[1,2], WANG Lu[1], JIANG Yang[1], MA Zi-Guang[1], WANG Wen-Qi[1,2], SUN Ling[1,2], JIA Hai-Qiang[1], WANG Wen-Xin[1], CHEN Hong*[1]

(1. Key Laboratory for Renewable Energy, Beijing Key Laboratory for New Energy Materials and Devices, Beijing National Laboratory for Condensed Matter Physics, Institute of Physics, Chinese Academy of Sciences, Beijing 100190, China;
2. University of Chinese Academy of Sciences, Beijing, 10049, China)

Abstract: Recently, a high localized carrier extraction efficiency and increasing of absorption coefficient was observed in low-dimensional semiconductors within a PN junction. Such phenomenon provides the possibility of fabricating novel high performance quantum well interband transition detector. In this work, we report the performance of the first photon detector based on the interband transition of strained InGaAs/GaAs quantum wells. The external quantum efficiency of the device was measured to be 31% using an absorption layer with only 100nm effective thickness and without an anti-reflection layer. Using such high value of quantum efficiency, an absorption coefficient of 3.7×10^4 cm^{-1} is calculated, which is obviously larger than previously reported values. The results here demonstrate the possibility of fabricating high performance and low cost infrared photon detectors.

Key words: InGaAs/GaAs, interband transition, photon detector
PACS: 72.80.Ey, 81.07.St, 85.60.Gz

基于量子阱带间跃迁的红外探测器原型器件

刘 洁[1,2], 王 禄[1], 江 洋[1], 马紫光[1], 王文奇[1,2], 孙 令[1,2], 贾海强[1], 王文新[1], 陈 弘*[1]
(1. 中国科学院物理研究所,北京凝聚态国家实验室,北京新能源材料与器件重点实验室,清洁能源重点实验室,北京 100190;
2. 中国科学院大学,北京 100049)

摘要:近期,实验发现PN结中局域载流子具有极高提取效率,并导致吸收系数的大幅度增加.文中报道基于上述现象的新型量子阱带间跃迁红外探测器原型器件的性能.利用含有InGaAs/GaAs多量子阱的PIN二极管,在无表面减反射膜的实验条件下,利用仅100 nm的有效吸收厚度,实现了31%的外量子效率.基于该数值推算得到,量子阱的光吸收系数达3.7×10^4 cm^{-1},该数值高于传统透射实验测量结果一个数量级.上述实验结果指出,利用量子阱带间跃迁工作机制,有望实现新颖的器件结构设计和提高现有器件性能.

关 键 词:铟镓砷/砷化镓;带间跃迁;光子探测器

中图分类号:TN362,O471.1　　**文献标识码**:A

Introduction

The working wavelength and dark current are two important figures of merits for photo detectors. Unfortunately, they are difficult to balance during the design of devices, especially for the ones working at infrared spectrum[1-3]. The working wavelength of a detector is decided by the bandgap of the material used in the absorption region. To detect an infrared photon, the bandgap of absorption layer should be narrow. However, higher thermal generation rate of narrow band gap material used in the infrared detection makes the dark current of detector larger than the visible light detector, such as HgCdTe, InSb, and InAs/GaSb type Ⅱ superlattice[4-8]. Even worse, photodiodes with working wavelength longer than 3 μm often works at low temperature to maintain a good signal to noise ratio[9-12]. The cooling system not only increases the cost, but also deteriorates other system per-

Received date: 2016-08-23, **revised date**: 2016-12-13　　**收稿日期**:2016-08-23, **修回日期**:2016-12-13
Foundation items:Supported by the National Natural Science Foundation of China (11574362, 61210014, 11374340, and 11474205), Innovative Clean-Energy Research and Application Program of Beijing Municipal Science and Technology Commission (Z151100003515001)
Biography:LIU Jie(1992-), female, Chongqing China, Ph. D. Research field is infrared detector. E-mail: liujie@iphy.ac.cn
* **Corresponding author**:E-mail:hchen@iphy.ac.cn

formance, such as the life time, size and weight[13-15].

Semiconductor quantum wells (QWs) are good candidate to provide both longer absorption wavelength and lower dark current. Infrared detector based on inter-subband transition in QWs, so called quantum well infrared detector (QWIP), was intensively studied over past decades[16-18]. However, the operating temperature of QWIP is still low due to the lower quantum efficiency and the bounded state to quasi-continuum state working mode[19-20]. The use of interband transition of QWs could lead to a higher performance. As shown in Fig. 1, a much lower noise level can be anticipated when most of the device is composed with wide band gap barrier material. The light absorption can be realized using narrow bandgap QW absorption layer. In such structure, the amount of thermal generated carriers can be largely suppressed due to the thinner narrow gap material layers than the conventional ones.

The problems of this strategy are obvious. Firstly, photon generated carriers can only enter the continuum state through thermionic emission and thermal assisted tunneling[21-23]. So the external quantum efficiency (EQE) could be low in those devices. Secondly, for most direct band gap semiconductor material, the absorption coefficient is around 10^3 cm^{-1} near its bandgap[24]. That requires an absorption thickness of several micrometers. For indirect band gap material, like Si, this value goes several tens of micrometers[25]. However, only finite epitaxy thickness of mismatch layer can be grown to avoid the misfit defects, typically in the nanometer range[26-28]. The misfit defects considerably deteriorate the device performances.

Recently, a high efficient optical generated carrier escape phenomenon of localized carriers within a PN junction was observed[29]. The carrier extraction ability of quantum dots (QDs) within a PN junction can reach as high as 88%. An obvious increase in absorption coefficient in the QDs within a PN junction was also noted, although the mechanism behind such phenomenon is still under study. The abnormal high carrier extraction efficiency of localized carrier and increasing in absorption coefficient perfectly solute the above mentioned two obstacles for the application of interband transition of QWs into photon detectors. Such results provide the possibility to fabricate new high performance photo detectors based on interband transition of low dimensional hetero structures.

In this work, we report the first prototype photon detector based on interband transition of InGaAs/GaAs QWs. With PN junction modulated absorption coefficient and carrier extraction from QWs, EQE up to 31% was obtained using only 20 periods of 5 nm InGaAs QWs without antireflection coating layers. The absorption coefficient calculated reaches as high as 3.7×10^4 cm^{-1}, around one order of magnitude higher than that in the conventional structure. Room temperature detectivity of the device reaches as high as $D^* = 1.43 \times 10^{13}$ cm $\sqrt{HZ}/W$.

1 Experimental

1.1 Material epitaxy

20-layer InGaAs/GaAs QW structures were grown by a solid-source VG-80H molecular beam epitaxy system on semi-insulating GaAs (001) substrates. Ten QW layers with deposition thicknesses of 5nm were embedded in the middle of a 50-nm-thick intrinsic GaAs barrier layer. After the deposition of the GaAs buffer and GaAs n^+ emitter, the rotated substrate temperature was reduced from 580°C to 480°C and maintained at 480°C until the end of the growth. The Si doping concertation of the n electrodes was $N_D = 3 \times 10^{18}$ cm^{-3}, and the Si doping concertation of the field damping layer inserted into the structure was $N_D = 6 \times 10^{17}$ cm^{-3}. The Be doping concentration of the p electrodes was $N_A = 3 \times 10^{18}$ cm^{-3}, and the Be doping concentration of the field damping layer inserted into the structure was $N_A = 3 \times 10^{17}$ cm^{-3}.

1.2 Device fabrication

The samples were fabricated by patterning the sample using photolithography and wet etching to achieve mesa isolation and expose the n-GaAs buffer. The mesa area was 1 mm^2. The electrodes of Ti/Au (20/100 nm) were deposited onto the p-GaAs in sequence by electron-beam evaporation. Then, 15/101/26/26/100-nm-thick Ni/Au/Ge/Ni/Au layers were deposited onto the n-GaAs for an n-ohmic contact. A wire bonding system was implemented with Si/Al wire on the electrodes.

1.3 PL (photo luminescence), PC (photo current) and external quantum efficiency (EQE) tests

The hypothermia photoluminescence intensities of the samples were measured with devices mounted in a closed-loop He-gas cryostat to maintain a stable temperature of 150 K. To achieve non-resonant excitation of the electrons in InGaAs QWs, a 905 nm semiconductor laser diode was used. The laser incident angle was ~30°. A beam chopper with a frequency of 1000 Hz was set up behind the laser. A condenser lens was placed in front of the cryostat to converge the spot. A neutral optical attenuator was used to adjust the excitation power. The PL signal normal to the sample was modulated by a triple-grating 50-cm monochromator prior to the analog lock-in amplifier (Stanford Research Systems model 830) and then detected by an InGaAs detector.

Since a laser was used to measure the EQE of the devices, EQE can be easily calculated based on the ratio of the photon number of testing laser with certain power and electron numbers of corresponding photo current.

The electrical properties of the devices were measured using Keithley 4200-scs semiconductor characterization system.

2 Results and discussion

The basic structure of our material is shown in Fig. 1(a). The optical property of this detector was evaluated using PL measurement, and the results are shown in Fig. 1(b). Due to the Stokes shift, PL may not clearly reveal the absorption peak of the QWs[30-32]. So photocurrent (PC) spectrum measurements on the QW sample were conducted, and the result is also shown in Fig. 1 (b). The main PL peak located at 956 nm, and the shoulder peak at 869 nm was attributed to the bulk GaAs. For the PC spectrum, a shoulder peak located at long wavelength

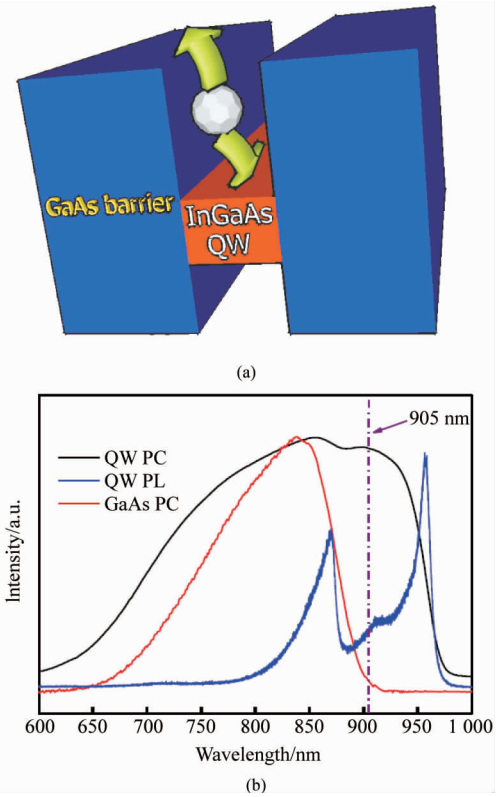

Fig. 1　(a) Schematic drawing of the working principle of the interband transition QW photon detector, (b) PL and PC spectra of InGaAs/GaAs QW photodiode measured at room temperature. PC spectrum of bulk GaAs photodiode was also shown as a reference curve

图 1　(a)带间跃迁量子阱光子探测器的工作原理示意图,(b)铟镓砷/镓砷量子阱探测器在室温下的光致发光和光电流谱. 镓砷体材料光电二极管的光电流谱也标注在示意图中

side of the GaAs absorption band was observed which was attributed to the InGaAs QW. A clear blueshift (from 956 nm to 896 nm) of the PC peak comparing with the PL peaks due to the Stokes shift was observed. In order to eliminate the PC contribution from bulk GaAs, another PC curve of bulk GaAs PIN diode was also shown in Fig. 1(b). At 905 nm, PC value of GaAs bulk is only 4% of its peak value.

Due to the PL peak of the device located near to the test laser peak (905 nm), clear localized carrier escape phenomenon cannot be observed under resonant excitation PL experiment. In Fig. 2 (a), we show a reference sample with similar structure compared with our device but higher In composition in the InGaAs QWs. Under 905 nm illumination, carriers can only be excited in InGaAs QWs. A variable resistor was connected to the circuit to adjust the current. A clear decrease of PL intensity with increasing current was observed. 81.4% PL intensity quenched from open circuit to short circuit condition.

In order to confirm that the localized photo excited carriers does form the current, the responsibility test of the detector was carried out using a 905 nm laser. Figure 2 (b) shows the *I-V* curves of the detector measured under illuminance and dark condition. The photovoltaic effect can be clearly seen. Such experimental results confirmed the high efficient photon excited carrier extraction from QWs into the continuum states.

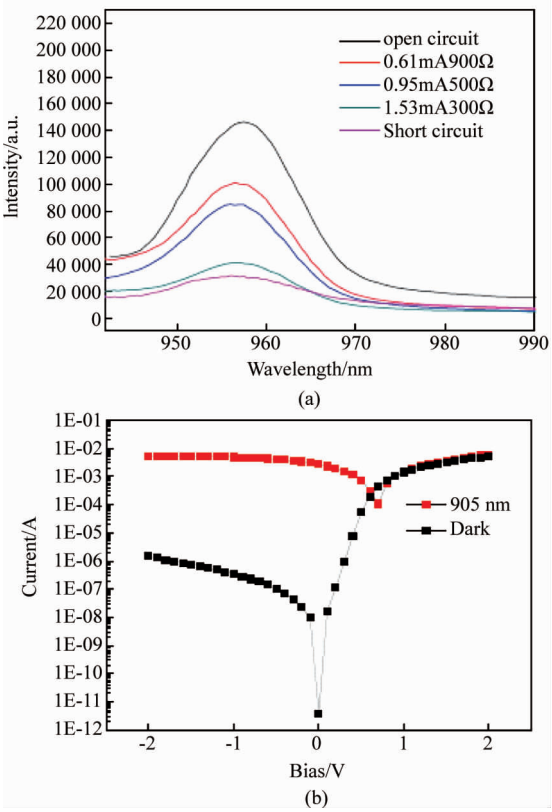

Fig. 2　(a) PL spectra of InGaAs/GaAs QWs measured under different circuit current, (b) Current-bias curves of InGaAs/GaAs QW photo diode measured under 905 nm illumination and dark condition

图 2　(a)不同短路电流下的光致发光谱,(b)905 nm 激光器下的电流电压曲线以及暗电流曲线

The photon generated current saturated at around -0.7 V which suggests the depletion region covers the QW thickness at this bias. At -1 V, the dark current density was measured to be 1.34×10^{-4} A/cm^2. Although no passivation layer was coated, this value is still higher than our expectation since our device is based on GaAs substrate. To check the origin of the dark current, another detector with 10 periods of InGaAs QWs was fabricated. The dark current decreased to 5.31×10^{-5} A/cm^2. Such result confirmed main dark current component was relevant to the strain relaxation induced defects. So possible higher performance could be anticipated when the material system changed to InGaAs/InP or InGaAs/InAlAs/InP QW with zero lattice mismatch[27, 33].

Because the absorption thickness was reduced to only 100 nm in the device, much shorter than the conventional 1 ~ 3.5 μm thickness, the dynamic range of the detector might change due to the band filling effect[34]. The EQE was measured at different incident light power, and the results are shown in Fig. 3. No EQE loss was observed for light power up to 5 W/cm^2, which was lim-

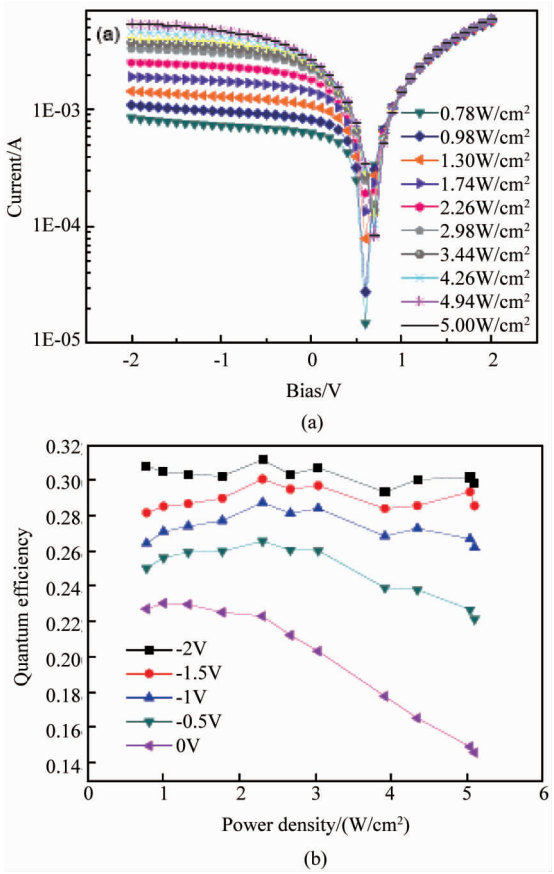

Fig. 3 The dependencies of (a) the current-bias curve and (b) the quantum efficiency of the InGaAs/GaAs quantum well photodiode on the illumination power
图3 (a)不同光照强度下的电流电压曲线;(b). 不同光功率密度下的量子效率

ited by our laser power. This value is far from enough for most application, such as fiber communication.

At low bias range, EQE reduces with increasing power, but stays constant once the bias is higher than 0.7 V. Such phenomenon can be explained by the large absorption coefficient of the QWs. At low bias range, when the incident power is relative low, most of the photons are absorbed by the first few QWs which located within the depletion region. Nevertheless, if the incident power gets higher, those QWs absorption is saturated. QWs located outside of the depletion region can neither provide enough free carriers nor efficiently provide electrical field to extract the free carriers. High EQE can only be realized by larger reverse bias. Such assumption can be verified by the around 0.7 V saturated bias in Figs. 2 ~ 3.

EQEs were calculated to be around 27% at -1 V and 31% at -2 V. Those values are quite high considering only 100 nm absorption thickness was used and no anti-reflection coating was deposited. Actually, around 40% light power reflection was measured with our device. Considering that the dynamic range of our detector is high enough for most application, much higher performance can be anticipated when the anti-reflection coating is used.

The absorption coefficient was calculated to be 3.1×10^4 cm^{-1} and 3.7×10^4 cm^{-1} at -1 V and -2 V, respectively, according to Eq. (1),

$$\eta = 1 - e^{-\alpha t} \quad , \quad (1)$$

where η is the EQE, α is the absorption coefficient and t is the absorption thickness. Those values are largely underestimated since the absorption coefficient is calculated through EQE. Surface reflection is neglected and the extraction efficiency of carriers from PN junction depletion region to external circuit is treated as 100%. Even through, such values is considerably larger than the values measured using transmission experiments[24]. The absorption coefficient varies with bias. Thus even larger value can be anticipated under optimized PN junction parameters and device fabrication process. In Table 1, we compared the absorption coefficient of our device with other PIN diodes consisting of vary materials working at different wavelength. A dramatic increasing of the absorption coefficient in the interband transition QW PIN diode can be seen. The 3.7×10^4 cm^{-1} value is one order of magnitude higher than the common PIN diodes and even a little bit higher than the devices with distributed Brag reflectors or resonant cavity structures.

The increased absorption coefficient can be understood as follows. The absorption coefficient of direct transition in the semiconductor can be written as the form in Eq. (2)[35].

$$a(\lambda) = \frac{2\pi\lambda}{c} | < 0 | \sigma | 0, n > |^2 S_n(E) \quad , \quad (2)$$

where λ is the wavelength of incident light, S_n is the density of state of $|0, n>$ per unit energy range near energy E, and c is the speed of light. Near the bandgap, the filling state of S_n can largely influence the absorption coefficient. Under common transmission measurement configuration, only recombination can consume the photo excited carriers. However, when the absorption coeffi-

Table 1 Absorption coefficient of PIN diodes working at different wavelength
表1 不同工作波长的PIN二极管的吸收系数

Ref	Absorption layer thickness/μm	Wavelength/μm	Absorption material	EQE	Absorption coefficient/cm^{-1}
37	0.65	0.85	Bulk GaAs	50% (90% with DBR)	$1.1 \times 10^4 (3.5 \times 10^4)$
38	1.5	1.19	Bulk InGaAsP	48%	4.4×10^3
39	~0.524	5.4	InAs/GaSb super lattice	17%	3.6×10^3
40	2	3.7	InAsSb	24%	1.4×10^3
41	1.5	2.23	InGaAs/GaAsSb type II QW	43% (200K,)	3.7×10^3
42	0.4676	1.55	Bulk InGaAs	80% (Resonant cavity enhanced)	3.4×10^4
Our work	0.1	0.905	InGaAs QW	31%	3.7×10^4

cient is deduced from the converting efficiency, both recombination and circuit current empty the energy band. Such effect would obviously increase the absorption coefficient. So, in Table 1, the calculated lower absorption coefficient among the literature may be resulted by the thicker absorption layer thickness. Such assumption consists with the large absorption coefficient value measured through EQE in GaAs/AlGaAs QWs[36].

So, if the absorption coefficient is relevant to the circuit current, it is no longer a material intrinsic parameter. Considering no anti-reflection layer was coated and there is still room for the material and device fabrication optimizations, absorption coefficient value higher than 10^5 cm^{-1} can be anticipated. This would require an absorption thickness less than 100 nm. Such an epitaxy thickness would facilitate many large mismatch material systems.

As indicated by Antoni Rogalski, the ratio of absorption coefficient to the thermal generation rate α/G_{th} is the fundamental figure of merit of any material for infrared photodetectors, which directly determines the detectivity limits of the devices[9]. The large absorption coefficient and lower thermal generation rate provided by the massive using of wide bandgap material not only provide a cost-effective method to fabricate photon detectors, but also are important to fabricated novel light-to-electricity converting devices, like solar cell.

Detectivity is another important figure of merit of the photon detectors. The Johnson noise, which limits D^* of our interband transition QW detector, is calculated by the following relation,

$$D^* = \frac{\eta(eA/I_d)}{hv} \quad , \quad (3)$$

in which η is the quantum efficiency, A is the effective area of our device, h is the Planck constant, ν is the frequency of the incident photon, and I_d represents the dark current. The calculated bias dependence of D^* is shown in Fig. 4. The peak detectivity is $D^* = 1.43 \times 10^{13}$ cm/W at zero bias when using the 905 nm laser with no antireflection layers and passivation layers.

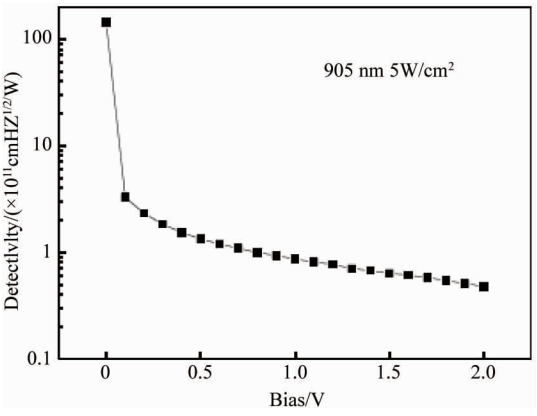

Fig. 4 Room temperature detectivity of the InGaAs/GaAs photodiode measured at different bias

图 4 不同偏压下的 InGaAs/GaAs 光电二极管室温探测率

InGaAs/GaAs QW material system was chosen because the mature epitaxy and device fabrication process. Although the detector demonstrates a cut-off wavelength of 896 nm, the prototype photon diode presented in this work demonstrates a prospective strategy for the design and fabrication of novel infrared detectors with high performance. For one example, the replacement of InGaAs/InAlAs or InGaAs/InP QW to the bulk InGaAs/InP based 1.3 ~ 1.55 μm detector may bring about a lower dark current, shorter carrier drifting time and lower cost. For another example, the operating temperature for InSb or HgCdTe based 3 ~ 5 μm detectors is typically 77 K or 60 K. The use of InGaSb/GaSb or InAsSb/GaSb QWs interband transition detector may dramatically increase the operating temperature through reducing the dark current.

3 Conclusion

In summary, the performance of a prototype photon detector based on interband transition of InGaAs/GaAs QW was reported. EQE reaches as high as 27% and 31% at -1 V and -2 V, respectively, with no anti-reflection layer coated. The calculated absorption coefficient reaches 3.7×10^4 cm^{-1} which is obviously higher than previously reported values. Such result demonstrates the possibility to fabricate novel high performance photon detectors based on interband transition of QW.

References

[1] Qiu W, Hu W, Lin C, . *et al*. Surface leakage current in 12.5 μm long-wavelength HgCdTe infrared photodiode arrays [J]. *Opt. Lett.* 2016, **41**(4), 828 - 831.

[2] Bai Z Z, Xu Z C, Zhou Y, *et al*. 320 x 256 dual-color mid-wavelength infrared InAs/GaSb superlattice focal plane arrays [J]. *Journal of Infrared and Millimeter Waves*, 2015, **34**(6), 716 - 720.

[3] Zhou Y, Chen JX, Xu Z C, *et al*. High performance long wavelength superlattice photodetectors based on be doped absorber region [J]. *Chinese Physics Letters*, 2014, **31**(10).

[4] Rogalski A, Antoszewski J, Faraone L. Third-generation infrared photodetector arrays [J]. *Journal of Applied Physics*, 2009, **105**(9): 091101.

[5] Qiu W C, HU W D. Laser beam induced current microscopy and photocurrent mapping for junction characterization of infrared photodetectors [J]. *Science China Physics, Mechanics & Astronomy*, 2015, **58**(2): 27001 - 027001.

[6] Hu W D, Liang J, Yue F Y, *et al*. Recent progress of subwavelength photon trapping HgCdTe infrared detector [J]. *Infrared Millim. Waves*. 2016, **35**(1): 25 - 36.

[7] Liu D, Lin C, Zhou S M, *et al*. Ohmic contact of Au/Mo on $Hg_{1-x}Cd_xTe$ [J]. *Journal of Electronic Materials*. 2016, **45**(6): 2802 - 2807.

[8] Ye Z H, Zhang P, Li Y, *et al*. Design of spectral crosstalk suppressing structure in two-color HgCdTe infrared focal plane arrays detector [J]. *Optical and Quantum Electronics*, 2014, **46**(10): 1283 - 1289.

[9] Rogalski A. Infrared detectors: status and trends [J]. *Progress in Quantum Electronics*, 2013, **27**(2-3): 59 - 210.

[10] Maimon S, Wicks G W. nBn detector, an infrared detectors with reduced dark current and higher operating temperature [J]. *Applied Physics Letters*, 2006, **89**(15), 151109.

[11] Chakrabarti S, Stiff-Roberts A D, Bhattacharya P, *et al*. High-temperature operation of InAs-GaAs quantum-dot infrared photodetectors with large responsivity and detectivity [J]. *IEEE Photonics Technology Letters*, 2004, **16**(5): 1361 - 1363.

[12] Zhou Y, Chen J, Xu Z, *et al*. Physics, Simulation, and Photonic En-

gineering of Photovoltaic Devices V [J], *Proceedings of SPIE*, 2016, Vol. 9743.
[13] Klipstein P C, Gross Y, Aronov D, *et al*. Infrared Technology and Applications XXXIX [J]. *Proceedings of SPIE*, 2013, Vol. 8704.
[14] Gravrand O, Destefanis G, Bisotto S, *et al*. Issues in HgCdTe research and expected progress in infrared detector fabrication [J]. *Journal of Electronic Materials*, 2013, **42**(11):3349-3358.
[15] Levenson E, Lerch P, Martin M C. Infrared imaging: Synchrotrons vs. arrays, resolution vs. speed [J]. *Infrared Physics & Technology*, 2006, **49**(1-2):45-52.
[16] Jing Y, Li Z, Li Q, *et al*. Angular dependence of optical modes in metal-insulator-metal coupled quantum well infrared photodetector [J]. *Aip Advances*, 2016, **6**(4).
[17] Lu W, Li L, Zheng H, *et al*. Development of an infrared detector: Quantum well infrared photodetector [J]. *Science in China Series G-Physics Mechanics & Astronomy*, 2009, **52**(7):969-977.
[18] Shi Z W, Wang L, Zhen H, *et al*. Molecular beam epitaxy growth of peak wavelength-controlled InGaAs/AlGaAs quantum wells for 4.3-μm mid-wavelength infrared detection [J]. *Nanoscale Res. Lett.*, 2013, **8**(1):1-5.
[19] Rogalski A. Quantum well photoconductors in infrared detector technology [J]. *Journal of Applied Physics*, 2003, **93**(8), 4355-4391.
[20] Levine B F. Quantum-well infrared photodetectors [J]. *Journal of Applied Physics*, 1993, **74**(8), R1-R81.
[21] Ridley B K. Hot electrons in low-dimensional structures [J]. *Reports on Progress in Physics*, 1991, **54**(2), 169-256.
[22] Luque A, Marti A. Photovoltaics towards the intermediate band [J]. *Nature Photonics*, 2011, **5**(3):137-138.
[23] Xu Z Y, Lu Z D, Yang X P, *et al*. Carrier relaxation and thermal activation of localized excitons in self-organized InAs multilayers grown on GaAs substrates [J]. *Physical Review B*, **54**(16): 11528-11531.
[24] Casey H C, Sell D D, Wecht K W. Concentration dependence of the absorption coefficient for n- and p-type GaAs between 1.3 and 1.6 eV [J]. *Journal of Applied Physics*, 1975, **46**(1):250-257.
[25] Green M A. Self-consistent optical parameters of intrinsic silicon at 300? K including temperature coefficients [J]. *Solar Energy Materials and Solar Cells*, 2008, **92**(11):1305-1310.
[26] Mooney P M, LeGoues F K, Tersoff J, *et al*. Nucleation of dislocations in SiGe layers grown on (001)Si [J]. *Journal of Applied Physics*, 1994, **75**(8):3968-3977.
[27] Jain S C, Willander M, Maes H. Stresses and strains in epilayers, stripes and quantum structures of III - V compound semiconductors [J]. *Semiconductor Science and Technology*, 1996, **11**(5):641.
[28] Dunstan D J, Young S, Dixon R H. Geometrical theory of critical thickness and relaxation in strained-layer growth [J]. *Journal of Applied Physics*, 1991, **70**(6):3038-3045.
[29] Wang W Q, Wang J L, Jiang Y, *et al*. Carrier transport in III - V quantum-dot structures for solar cells or photodetectors [J]. *Chin. Phys. B*, 2016, **25**(9):97307-097307.
[30] Fry P W, Itskevich I E, Parnell S R, *et al*. Photocurrent spectroscopy of InAs/GaAs self-assembled quantum dots [J]. *Physical Review B*, 2000, **62**(24), 16784-16791.
[31] Prins F E, Lehr G, Burkard M, *et al*. Photoluminescence excitation spectroscopy on intermixed GaAs/AlGaAs quantum wires [J]. *Applied Physics Letters*, 1993, **62**(12), 1365-1367.
[32] Talapin D V, Koeppe R, G? tzinger S, *et al*. Highly Emissive Colloidal CdSe/CdS Heterostructures of Mixed Dimensionality [J]. *Nano Letters*, 2003, **3**(12), 1677-1681.
[33] Ito H, Kodama S, Muramoto Y, *et al*. High-speed and high-output InP-InGaAs unitraveling-carrier photodiodes [J]. *IEEE Journal of Selected Topics in Quantum Electronics*, 2004, **10**(4), 709-727.
[34] Nelson D F, Gershenzon M, Ashkin A, *et al*. Band-filling model for GaAs injection luminescence [J]. *Applied Physics Letters*, 1963, **2**(9):182-184.
[35] Elliott R J. Intensity of optical absorption by excitons [J]. *Physical Review*, **108**(6):1384-1389.
[36] WoodT H. Direct measurement of the electric-field-dependent absorption coefficient in GaAs/ AlGaAs multiple quantum wells [J]. *Applied Physics Letters*, 1986, **48**(21):1413-1415.
[37] Gokkavas M, Dosunmu O, Unlu M S, *et al*. High-speed high-efficiency large-area resonant cavity enhanced p-i-n photodiodes for multimode fiber communications [J]. *IEEE Photonics Technology Letters*, 2001, **13**(12), 1349-1351.
[38] Xi S P, Gu Y, Zhang Y G, *et al*. InGaAsP/InP photodetectors targeting on 1.06? μm wavelength detection [J]. *Infrared Physics & Technology*, 2016, **75**: 65-69.
[39] Walther M, Schmitz J, RehmR, *et al*. Growth of InAs/GaSb short-period superlattices for high-resolution mid-wavelength infrared focal plane array detectors [J]. *Journal of Crystal Growth*, 2005, **278**(1-4):156-161.
[40] Shao H, Li W, Torfi A, *et al*. Room-temperature InAsSb photovoltaic detectors for mid-infrared applications [J]. *IEEE Photonics Technology Letters*, 2006, **18**(16), 1756-1758.
[41] Sidhu R, Ning D, Campbell J C, *et al*. A long-wavelength photodiode on InP using lattice-matched GaInAs-GaAsSb type-II quantum wells [J]. *IEEE Photonics Technology Letters*, 2005, **17**(12):2715-2717.
[42] Chen C H, Tetz K, Fainman Y. Resonant-cavity-enhanced p-i-n photodiode with abroad quantum-efficiency spectrum by use of an anomalous-dispersion mirror [J]. *Appl. Opt.* 2005, **44**(29):6131-6140.